

<https://doi.org/10.1038/s41540-024-00427-4>

# Tipping-point transition from transient to persistent inflammation in pancreatic islets

Check for updates

Thomas Holst-Hansen<sup>1,4</sup>, Pernille Yde Nielsen<sup>1,2,4</sup>, Mogens H. Jensen<sup>1</sup> ✉, Thomas Mandrup-Poulsen<sup>3</sup> ✉ & Ala Trusina<sup>1</sup> ✉

Type 2 diabetes (T2D) is associated with a systemic increase in the pro-inflammatory cytokine IL-1 $\beta$ . While transient exposure to low IL-1 $\beta$  concentrations improves insulin secretion and  $\beta$ -cell proliferation in pancreatic islets, prolonged exposure leads to impaired insulin secretion and collective  $\beta$ -cell death. IL-1 is secreted locally by islet-resident macrophages and  $\beta$ -cells; however, it is unknown if and how the two opposing modes may emerge at single islet level. We investigated the duality of IL-1 $\beta$  with a quantitative in silico model of the IL-1 regulatory network in pancreatic islets. We find that the network can produce either transient or persistent IL-1 responses when induced by pro-inflammatory and metabolic cues. This suggests that the duality of IL-1 may be regulated at the single islet level. We use two core feedbacks in the IL-1 regulation to explain both modes: First, a fast positive feedback in which IL-1 induces its own production through the IL-1R/IKK/NF- $\kappa$ B pathway. Second, a slow negative feedback where NF- $\kappa$ B upregulates inhibitors acting at different levels along the IL-1R/IKK/NF- $\kappa$ B pathway — IL-1 receptor antagonist and A20, among others. A transient response ensues when the two feedbacks are balanced. When the positive feedback dominates over the negative, islets transit into the persistent inflammation mode. Consistent with several observations, where the size of islets was implicated in its inflammatory state, we find that large islets and islets with high density of IL-1 $\beta$  amplifying cells are more prone to transit into persistent IL-1 $\beta$  mode. Our results are likely not limited to IL-1 $\beta$  but are general for the combined effect of multiple pro-inflammatory cytokines and chemokines. Generalizing complex regulations in terms of two feedback mechanisms of opposing nature and acting on different time scales provides a number of testable predictions. Taking islet architecture and cellular heterogeneity into consideration, further dynamic monitoring and experimental validation in actual islet samples will be crucial to verify the model predictions and enhance its utility in clinical applications.

When cells of higher eukaryotes respond to perturbations in cellular homeostasis, they often choose between two primary strategies: They either adapt and repair the inflicted damage or commit to programmed cell death. The final decision depends on the severity of damage as reflected in the intensity of activation of signaling pathways and levels of regulatory proteins. It becomes increasingly clear that the same proteins that act protectively under remediable stresses can induce cell death when cells face severe or prolonged stress.

Furthermore, the switch from adaptive to detrimental action is often sudden and irreversible<sup>1,2</sup>. The examples of life/death duality span across kinases (Ire1<sup>3</sup>, PERK<sup>4,5</sup>, JNK<sup>6</sup>), transcription factors (p53<sup>7,8</sup>), DNA repair proteins (BRCA1<sup>9</sup>), mitochondrial factors (Bax and Bak<sup>10</sup>), ROS signaling molecules (H<sub>2</sub>O<sub>2</sub><sup>11,12</sup>) and cytokines (IL-1<sup>13</sup>).

While the intracellular components of these life/death signals are involved in single-cell decisions, diffusible or secreted factors (e.g., H<sub>2</sub>O<sub>2</sub> and IL-1) are used in intercellular communication and influence collective

<sup>1</sup>Niels Bohr Institute, University of Copenhagen, Copenhagen, Denmark. <sup>2</sup>Department of Applied Mathematics and Computer Science, Technical University of Denmark, Lyngby, Denmark. <sup>3</sup>Department of Biomedical Sciences, Faculty of Health and Medical Sciences, University of Copenhagen, Copenhagen, Denmark. <sup>4</sup>These authors contributed equally: Thomas Holst-Hansen, Pernille Yde Nielsen. ✉ e-mail: [mhjensen@nbi.dk](mailto:mhjensen@nbi.dk); [tmpo@sund.ku.dk](mailto:tmpo@sund.ku.dk); [trusina@nbi.dk](mailto:trusina@nbi.dk)

decisions. There are several exciting findings uncovering the dynamical nature of the life/death transitions in single cells<sup>12</sup>; however, the understanding of protein duality at the tissue level remains an uncharted area. It is unclear how the geometry of the tissue and inflicted damage influence the collective decision.

We address these questions with the help of theoretical and in silico modeling of IL-1 $\beta$  regulation in islets of Langerhans. The dual mode of action of IL-1 $\beta$  cytokine on the pancreatic  $\beta$  cell is well established: while transient exposure to low IL-1 $\beta$  concentrations improves insulin secretion and promotes  $\beta$ -cell survival, prolonged exposure to high levels of IL-1 $\beta$ , as in chronic inflammation, leads to impaired insulin secretion and  $\beta$ -cell death<sup>14–17</sup>. The islets of Langerhans present a unique model system for quantitative understanding, as islet geometry and their cellular composition are well described across many species<sup>18–20</sup>, the IL-1 $\beta$  regulatory network is

well studied, and islets comprise a computationally amenable number of IL-1 $\beta$  secreting cells, (ISC,  $\beta$ -cells or macrophages).

Furthermore, IL-1 $\beta$  plays an important role in the progression of type 1 and 2 diabetes<sup>13,17</sup>. Type 2 diabetes results when pancreatic  $\beta$ -cells fail to compensate for increased insulin needs as a consequence of insulin resistance. T2D is associated with systemic low-grade chronic inflammation and immune-cell infiltration of insulin-sensitive tissues and pancreatic islets. Proof of concept of the role of IL-1 in the progression of T2D stems from clinical trials, where attenuating IL-1 signaling improves glycemia by enhancing  $\beta$ -cell function<sup>21,22</sup>. Interestingly, both infiltrating macrophages and pancreatic  $\beta$ -cells are believed to be sources of IL-1 $\beta$  in pancreatic islets<sup>16</sup>. IL-1 $\beta$  synthesis is tightly regulated and requires two signals (Fig. 1A). A priming signal (Signal 1), in the form of pathogen-associated molecular patterns (PAMPS) and pro-inflammatory cytokines including IL-1 $\beta$  itself

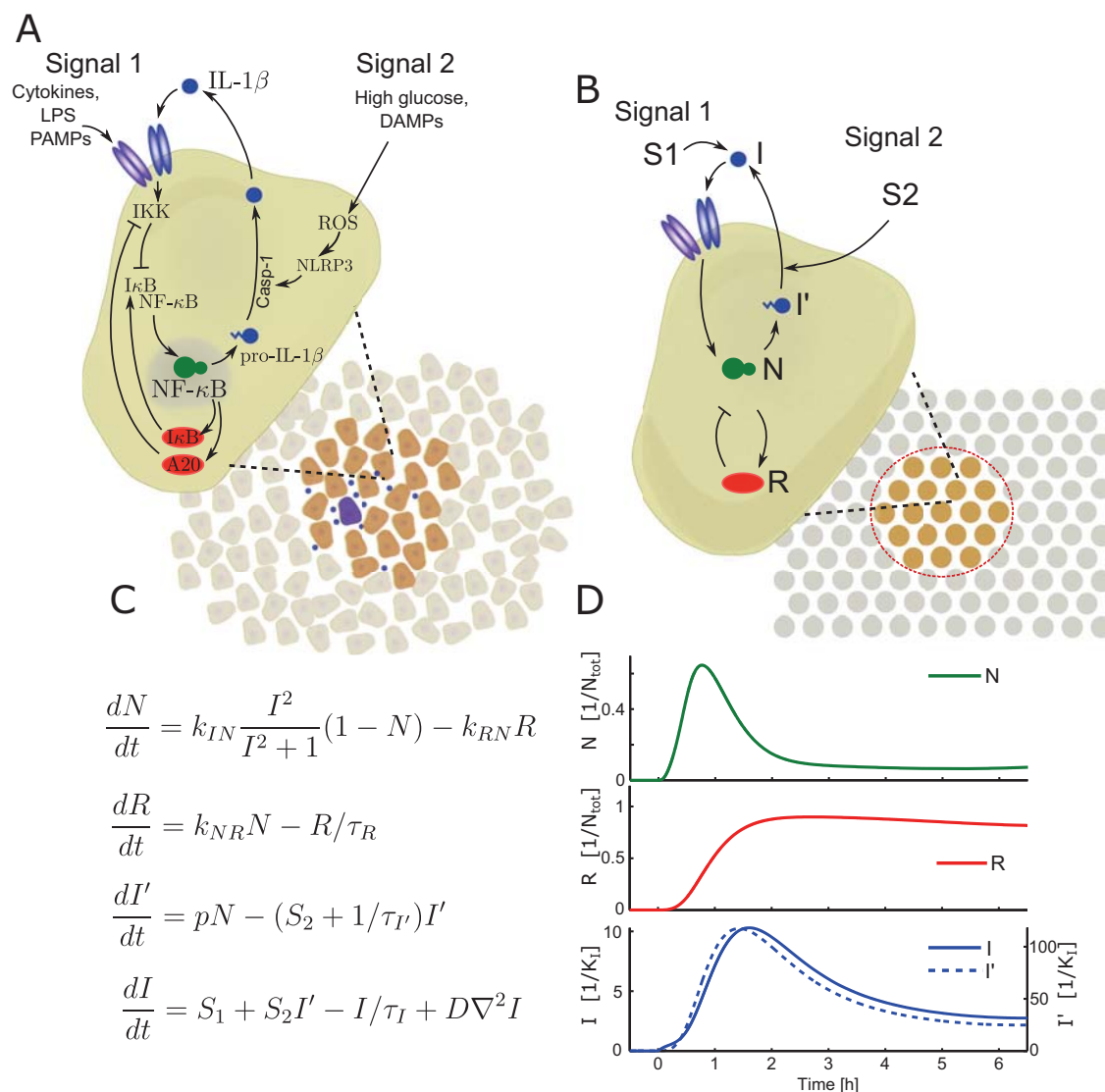


**Fig. 1 | Schematic of the IL-1 $\beta$  regulatory loops in a pancreatic islet and the corresponding in silico model. A** The main signaling pathways of IL-1 $\beta$  in a  $\beta$ -cell or immune cell infiltrating the islets. The regulatory system can be grouped into two pathways; Signal 1 leads to NF- $\kappa$ B activation and production of pro-IL-1 $\beta$ . Signal 2 activates the NLRP3 inflammasome and leads to subsequent caspase-1 activation that cleaves pro-IL-1 $\beta$  into mature IL-1 $\beta$ . Together Signal 1 and 2 compose a self-amplifying feedback loop by which IL-1 $\beta$  stimulates its own production. We model the islet of Langerhans in two dimensions as a cluster of IL-1-secreting cells, surrounded by non-secreting cells, which do not respond to IL-1 $\beta$ . In the model a random set of cells act as initial sources of Signal 1. **B** Simplified model of the IL-1 $\beta$

signaling pathways in a single cell. The model includes four variables representing pro-IL-1 $\beta$  ( $I'$ ), IL-1 $\beta$  ( $I$ ), NF- $\kappa$ B ( $N$ ) and proteins regulating NF- $\kappa$ B through negative feedback loops (grouped into the variable  $R$ ). There are two free parameters in the model:  $S_1$  represents stimuli by a cytokine source (e.g., IL-1 $\beta$ ) and is related to Signal 1 and  $S_2$  is the maturation rate of IL-1 $\beta$  that is related to caspase-1 activity and hence Signal 2. **C** Model equations describing IL-1 $\beta$  dynamics. **D** The output from a single IL-1 secreting cell is fitted to NF- $\kappa$ B data such that the typical NF- $\kappa$ B response peaks within  $\approx$  1 h of stimulus. Here we show the response of a single cell stimulated by a persistent  $S_1 = 5.0 \text{ h}^{-1}$  and  $S_2 = 0.5 \text{ h}^{-1}$ .

activates NF-κB, which in turn induces expression of the IL-1β precursor pro-IL1β. This is an inactive form of IL-1β that remains inside the cell. A second signal (Signal 2), represented by high concentrations of glucose and free fatty acids (FFA) and Damage Associated Molecular Patterns (DAMPS), activates the NLRP3 inflammasome for pro-IL-1β cleavage by caspase-1. This converts pro-IL-1β into its mature form, which is exported into the extracellular space<sup>15</sup>. Exposure of β-cells to both Signal 1 and Signal 2 results in an amplifying feedback loop in which IL-1β induces its own expression. As a result, the β-cells may contribute to chronically elevated IL-1β levels in a self-sustaining manner establishing a vicious cycle<sup>13,14,23</sup>. If this auto-stimulation is not balanced, it may result in chronic inflammation and cause islet pathology and eventual death. Furthermore, IL-1β acts as a chemoattractant for immune cells such as macrophages. The attracted macrophages may further contribute to the chronic levels of IL-1β in the inflamed islets, as the macrophages use the same set of cues as β-cells to upregulate mature IL-1β.

In spite of the potential importance of IL-1β in T2D progression and the extensive knowledge of IL-1β regulation in pancreatic β- and immune cells, the nature of IL-1β transition from an adaptive to a deleterious state remains largely unknown. It is not known if the transition in single islets is gradual, with a gradually increasing fraction of dysfunctional cells, or if it is a collective decision, with all cells transitioning from a functional to dysfunctional state simultaneously. Remarkably, islet geometry correlates with sensitivity towards inflammation: the immune cells infiltrate *large* islets first<sup>15</sup>; large islets are underrepresented in T2D patients<sup>24</sup> and knocking down the NLRP3 inflammasome in murine models of T2D caused a significant increase in islet sizes compared with wildtype obese mice<sup>25</sup>. To date, the mechanisms behind the correlations between islet geometry and its propensity to inflammation are unclear. Interestingly, recent studies have shown that waves of increased cytosolic Ca<sup>2+</sup> – a critical signal in the stimulus-secretion coupling that triggers insulin granule exocytosis – are initialized by individual β-cells and then spreads across the pancreatic islets<sup>26</sup>. These findings identify “leader” and “follower” cells, indicating that β-cells in pancreatic islets display collective behaviors initialized by single cells.

With the help of the *in silico* model, we find that when islets are exposed to pro-inflammatory and nutritional cues, there are two characteristic modes of IL-1 upregulation: *transient* or *persistent*. More importantly, the model predicts that while the increase in the number of pathological islets exposed to pro-inflammatory and nutritional cues may be slow and gradual, the transitions to the persistent mode in single islets are rapid and sudden. Our analysis shows that the transition is sensitive to islet architecture and size: while larger islets with dense cores of ISC are more prone to chronic inflammation, the small-sized and folded organization of human islets adds to the tight regulation of IL-1β and offsets the onset of the persistent mode.

## Results

### Mapping known IL-1 regulations to a mathematical model

In order to minimize the number of unknown parameters and variables, we aimed to construct a simple model, which captures the qualitative behavior of the biological system. In our earlier theoretical studies, we have shown that cytokine auto-stimulation through the NF-κB pathway belongs to a class of phenomena known as excitable media<sup>27–29</sup>. Here we modify an earlier model<sup>27,29</sup> to describe the NF-κB mediated inflammatory response in pancreatic islets. It has been shown that, in addition to macrophages, β-cells contribute to IL-1β accumulation in the islets<sup>30</sup>. In the current model, we do not differentiate between β-cells and macrophages, and refer to them as IL-1β Secreting Cells (ISC). We assume that other endocrine cell types (α, δ and γ) do not contribute to cytokine secretion.

A two-dimensional model was constructed in which cells were arranged on a hexagonal grid, and their positions were fixed. All cells inside a circular area in the middle of the hexagonal grid were modeled as ISCs representing a pancreatic islet (Fig. 2B). Cells outside the islet represented surrounding tissue in which IL-1β was allowed to diffuse and degrade. IL-1β

was assumed to diffuse freely between cells; based on a molecular weight of 17 kDa, the diffusion coefficient of freely diffusing IL-1β is estimated to be  $D = 20 \mu\text{m}^2/\text{s}$ <sup>31</sup>. While we do not explicitly model small blood vessels penetrating into islets, we account for the fact that β-cells are typically in close vicinity to the blood, by using plasma clearance rates of IL-1β as an estimate of the effective IL-1β half-life in the islets ( $\tau_I = 0.17 \text{h}$ )<sup>32</sup>. The choice of these and other parameters are summarized in Table 1, “Methods”.

The individual ISCs were modeled as entities that were able to both sense surrounding levels of IL-1β and to secrete IL-1β into the extracellular space. We reduced the detailed regulatory network of IL-1β, shown in Fig. 1A, to an effective regulatory network (Fig. 1B). The model includes four rescaled dynamic variables:  $I$ ,  $I'$ ,  $N$  and  $R$  (see details about rescaling in “Methods”).  $I$  represents the concentration of IL-1β,  $I'$  is the concentration of pro-IL-1β,  $N$  represents the concentration of nuclear NF-κB (i.e., active in transcription), and  $R$  represents the combined effect of regulating proteins that inhibit active NF-κB (e.g., IκBa, A20, cylindromatosis (CYLD), etc.). While the IκBa negative feedback is significantly faster, compared to A20 and CYLD, combining them together in one slow feedback produces qualitatively the same results as long as one does not aim to reproduce the lower amplitude secondary oscillations<sup>27</sup>.

The model for an ISC is therefore a system of ordinary differential equations together with a partial differential equation for IL-1β:

$$\frac{dN}{dt} = k_{IN} \frac{I^2}{I^2 + 1} (1 - N) - k_{RN} R \tag{1}$$

$$\frac{dR}{dt} = k_{NR} N - R/\tau_R \tag{2}$$

$$\frac{dI'}{dt} = pN - \left( S_2 + \frac{1}{\tau_{I'}} \right) I' \tag{3}$$

$$\frac{dI}{dt} = S_1 \delta(\{x_i\}) + S_2 I' - \frac{I}{\tau_I} + D \nabla^2 I \tag{4}$$

The two-dimensional model of a pancreatic islet is a reaction-diffusion model on a hexagonal grid. While the variable  $I$  is allowed to diffuse between cells, the variables  $N$ ,  $R$  and  $I'$  are local intracellular variables. Only the cells representing ISCs in the pancreatic islet are able to synthesize *de novo* IL-1. This is modeled by setting the parameter  $p$  to a positive value for ISCs cells and to zero for all non-ISCs.

The first two equations governing dynamics of NF-κB activation and inhibition (Fig. 1D) focus on capturing the characteristic initial peak in NF-κB response and were first introduced in our earlier work<sup>27,29</sup>.

The parameters  $k_{IN}$ ,  $k_{RN}$ ,  $k_{NR}$  and  $\tau_R$  have been fixed by fitting the model to experimental data for TNF-induced NF-κB dynamics in single cells<sup>33</sup>, such that the timing of the initial peak in NF-κB activation matched experimentally observed values<sup>27,29,33</sup> (see “Methods” for details of fitting).

While the data on IL-1β induced NF-κB responses in single cells is not available; population-averaged data supports transient activation of NF-κB with a peak around 2 h<sup>34</sup>.

The last two equations and parameters  $p$ ,  $S_1$ ,  $S_2$ ,  $\tau_I$ ,  $\tau_{I'}$  and  $D$  are related to the dynamics (production, degradation and diffusion) of IL-1β. Our investigation focuses on the parameters  $S_1$  and  $S_2$ , related to the levels of initiating inflammatory (Signal 1) and metabolic cues (Signal 2), and how these parameters affect the dynamics of the model. Further details on model parameters and approximations are presented in detail in Table 1 in the “Methods” section.

Although IL-1β could be produced solely by islet-invading immune cells such as macrophages, it has been hypothesized that the initial increase of IL-1β is mainly produced by stressed β-cells. This increase may subsequently attract immune cells, adding further to the increasing levels of IL-1β<sup>14</sup>. In our model, we do not specify the originators of the initial increase of IL-1β, but simulate Signal 1 by adding an additional production of IL-1β (the term  $S_1 \delta(\{x_i\})$  in Eq. (4)) to a number of randomly chosen ISCs within the

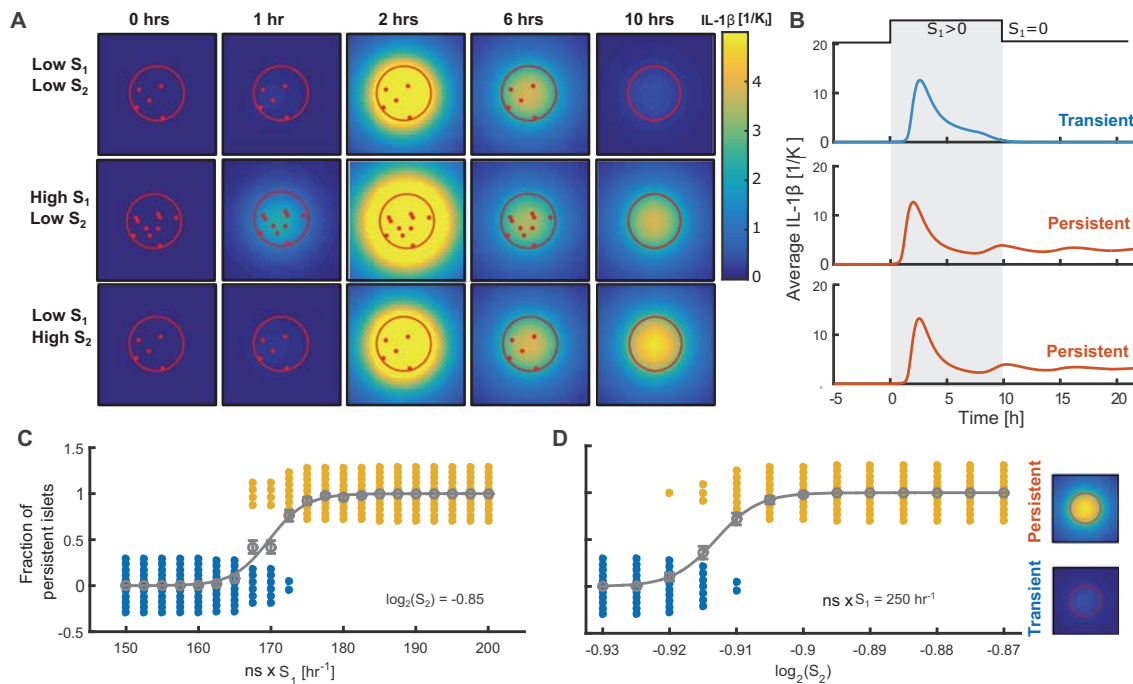


**Fig. 2 | Transient and persistent IL-1 modes emerge in single islets.** **A** Snapshots of simulated IL-1 dynamics in an islet in response to different combinations of high and low  $S_1$  (Signal 1) and  $S_2$  (Signal 2). All cells within the red circle are modeled as ISCs (intra-islet cells), and outside of the circle as non-secreting cells (surrounding tissue cells). Only the  $S_1$  sources cells (red dots) have non-zero values of  $S_1$  between 0 and 10 h (B, top panel). **B** Time courses of IL-1 $\beta$  averaged over all cells in the islet corresponding to the islets in (A). The gray area indicates the time interval in which the  $S_1$  sources are “tuned on”. Under all conditions, the islet displays an initial strong secretion of IL-1 $\beta$  peaking after ~2 h. At low  $S_1$  and  $S_2$  (top panel), the islet responds transiently and will return to the resting state (Supplementary Movie 1). If either  $S_2$  or  $S_1$  is high (middle and bottom panel), the islet enters a persistent (“locked”) state with sustained IL-1 $\beta$  expression (Supplementary Movies 2 and 3). **C, D** Probability of locking at different levels of  $S_1$  and  $S_2$ . The random position of  $S_1$  sources (indicated by red dots in A) introduces stochasticity in the islet fates (locking) for some

values of parameters  $S_1$ ,  $ns$  and  $S_2$  (see also Fig. 5D). Here, we show the results of 50 simulations with equal parameter values, but with different random positions of the  $S_1$  sources. The fraction of persistent islets increases with the total  $S_1$  dose (number of sources ( $ns$ ) times the  $S_1$ ) (C) and with increasing  $S_2$  (D). Gray points and error bars show the average number of persistent islets, gray line is a sigmoidal fit to the fraction of persistent islets, used to find  $EC_{50}$  (see “Methods”, Supplementary Note 4 and Supplementary Fig. S5). Overlaid in blue and yellow are the bee-swarm plots, where each dot represents five simulations (all yellow dots have a value of 1 and all blue dots have value of 0). The bee-swarm plots visualize that islets are in either transient (blue dots) or persistent (yellow dots) states, as indicated by the insert snapshots to the far right. For both parameter scans (C and D), there is a region of co-existence between persistent islets and transient islets that return to the resting state. The state of individual islets depends on the positions of  $S_1$  sources. Here each islet has a radius of 7 ISCs. Results for larger sizes are shown in Fig. 5.

islet. These cells thus become *sources of Signal 1*. As these cells are chosen at random, the positioning of these Signal 1 sources will be also random for each simulation. In Fig. 2A and throughout, the position of Signal 1 sources are indicated by red dots. The sources of Signal 1 act as initiators of the model, allowing us to study how the ISCs respond and regulate IL-1 $\beta$  when exposed to an external stimulus. While all the ISCs are able to produce and secrete IL-1 $\beta$ , only Signal 1 sources have non-zero value of the  $S_1$  parameter. Overall Signal 1 in the system is thus characterized by both the strength of basal IL-1 $\beta$  production,  $S_1$ , and the number of sources,  $ns$  (total *Signal 1 dose* is equal to  $S_1 \times ns$ ). We stress that the initial sources described by the  $S_1$  parameter reflect a cumulative effect of other NF- $\kappa$ B activating agents such as TNF, TLR, PAMPs or other cytokines, but for the purpose of our model, we describe these as IL-1 $\beta$  sources in order to minimize the number of variables. While we choose to model  $S_1$  as a few discrete sources, we have tested that the model results hold if, instead,  $S_1$  is equally distributed across all cells. This configuration is, in particular, relevant for cases where Signal 1 represents low-grade inflammation stemming from sources outside the islets, with low levels of pro-inflammatory cytokines circulating in the blood<sup>35</sup>.

The severity of T2D is positively correlated with the levels of glucose, the amount of free fatty lipids concentration in the blood and DAMPs in the extracellular space. These factors all contribute to the activity of the NLRP3 inflammasome and, in turn, caspase-1, see Fig. 1A. In order to construct a simple model, we merge the effects which contribute to an increased caspase-1 activity into the  $S_2$  parameter (see Fig. 1C). In our simulations  $S_2$  is

set to be the same for all ISC and does not change in time. But since caspase-1 actively cleaves pro-IL-1 $\beta$  into mature IL-1 $\beta$ , the closest biological interpretation of  $S_2$  is the activity of caspase-1.  $S_2$ , in combination with the production rate of pro-IL-1 $\beta$ ,  $p$ , constitutes the strength of the positive feedback by which  $\beta$ -cells amplify the local IL-1 $\beta$  concentration. This becomes a crucial parameter in the qualitative behavior of the simulated islets.

The ISCs synthesize IL-1 $\beta$  and secrete it into the extracellular space, where IL-1 $\beta$  acts in an autocrine and paracrine manner. In each simulation, islets are initiated in a steady state of low activity with no stimulation, i.e., NF- $\kappa$ B is inactive and  $S_1$  equals zero for all ISCs. At time zero the islets are stimulated by a number of small inflammation sources—technically  $S_1$  is set equal to a non-zero value for a discrete set of spatial positions. The sources are only non-zero for a finite time, after which the  $S_1$  parameter is set equal to zero, and we monitor the islet response. While the  $S_2$  parameter is non-zero at all times and for all ISCs (cells within the islet, indicated by a red circle in Fig. 2A), the  $S_1$  parameter is only non-zero for a discrete set of islet cells (indicated by red dots in Fig. 2A).

**The model predicts transient and persistent production of IL-1 $\beta$  in single islets, in correspondence with the IL-1 $\beta$  dual effect**

The bimodal effects of IL-1 on  $\beta$ -cell function and viability are associated not only with the concentration of IL-1 but also with the duration of exposure. Transient exposure leads to protective effects, while prolonged exposure promotes cell death<sup>14,36,37</sup>. As pancreatic islets have been shown to mount a

**Table 1 | Model parameters**

PARAMETER	VALUE	UNIT	NAME	REFERENCE
$k_{IN}$	5.0	$h^{-1}$	Rate of NF- $\kappa$ B induction	Hand-fitted to NF- $\kappa$ B activation from ref. 33.
$k_{RN}$	5.0	$h^{-1}$	Inhibition strength of inhibitor on NF- $\kappa$ B	Hand-fitted to NF- $\kappa$ B activation from ref. 33.
$k_{NR}$	1.4	$h^{-1}$	Combined transcription and translation rate of NF- $\kappa$ B inhibitor	Hand-fitted to NF- $\kappa$ B activation from ref. 33.
$\tau_R$	7.0	h	Half-life of combined NF- $\kappa$ B inhibitor	Variable R represents the combined effect of the “slow” negative regulators of the IL-1 $\rightarrow$ IKK $\rightarrow$ NF- $\kappa$ B pathway, e.g., IL-1RA and A20. The half-life of A20 protein is 8 h <sup>61</sup> , and it takes 12–24 h for IL-1RA to reach significant levels <sup>62</sup> in human monocytes. Note, $\tau_R$ in effect controls the speed of the negative feedback loop. The results will be qualitatively the same as long as the time-scales of the negative and positive feedbacks are “separated” ( $\tau_R$ is several-fold larger than $\tau_I$ and $\tau_I$ )
$p$	1400	$h^{-1}$	Combined transcription and translation rate of pro-IL-1 $\beta$	$p$ is part of the positive feedback of IL-1 $\beta$ onto NF- $\kappa$ B. We have chosen a fixed value, but $p$ can also be the free parameter instead of $S_2$ . $p$ sets the maximum secretion rate and must therefore be sufficiently high to get locked islet states.
$\tau_I$	2.0	h	Pro-IL-1 $\beta$ half-life	Half-life of the IL-1 $\beta$ mRNA 2–4 h in human epidermal keratinocytes <sup>63</sup> at least 2 h in human blood mononuclear cells <sup>64</sup> and 2.5 h in primary monocytes <sup>65</sup> .
$\tau_I$	0.17	h	IL-1 $\beta$ clearance rate	Clearance rate from ref. 66.
$D$	300	$cells^2 h^{-1}$	Diffusion constant	Diffusion constant normalized with respect to cell size. Cell size from ref. 33, diffusion constant from ref. 31.
$S_I$	free	$h^{-1}$	Rate of external stimulus	Inflammatory cue received outside the normal IL-1 $\beta$ production of islets.
$S_2$	free	$h^{-1}$	Combined maturation and secretion rate of IL-1 $\beta$	If we assume secretion is instantaneous, $S_2$ most closely corresponds to the rate caspase-1 cleaves pro-IL-1 $\beta$ into mature IL-1 $\beta$ .

significant local IL-1 response, among the endocrine islet cells and infiltrating macrophages, we wanted to investigate if the two distinct temporal profiles of IL-1 may emerge at the single islet level. To investigate this, we monitored how levels and duration of the IL-1 production depend on inflammatory Signal 1 ( $S_I$ ) and nutritional Signal 2 ( $S_2$ ) cues within an in silico islet.

We found that whereas low levels of  $S_I$  and  $S_2$  result in *transient* upregulation of IL-1 $\beta$ , high levels of either  $S_I$  or  $S_2$  (or both) will result in *sustained high* levels of IL-1 $\beta$  (Fig. 2A, B). When an islet with a low  $S_2$  is stimulated by a small number of inflammatory sources (low  $n_s$ ), it responds with a pulsating NF- $\kappa$ B activity and a similar pulsating amplification of IL-1 $\beta$  (Fig. 2A). Once the sources are removed, the islet stops pulsing and returns to the resting state (see Supplementary Movies 1 and 4). Hence, the islet exhibits a transient response to the transient inflammatory cues. If a similar islet is exposed to either higher Signal 1 (more initial sources of inflammation) or to higher Signal 2 (e.g., higher caspase-1 activity), the cells will collectively amplify the IL-1 $\beta$  concentration and transition into a “locked” state of constantly elevated IL-1 $\beta$  (see Supplementary Movies 2, 3, 5 and 6 and Supplementary Note 1). In this state, the islet will sustain the high levels of IL-1 $\beta$ , and will not settle back to the resting state—even when the initial IL-1 $\beta$  sources are removed. The locked state simulates a state of chronic inflammation, where prolonged exposure to high levels of IL-1 $\beta$  has been reported to have deleterious effects leading to impaired insulin secretion and  $\beta$ -cell death<sup>14–17</sup>. Similarly to our earlier work<sup>27,29</sup>, dynamical systems analysis showed that the locked state is a consequence of an over-active positive feedback in ISCs, which prevents the fast variables (I, I' and N) from undergoing a saddle node bifurcation and return to low cytokine levels. These results are consistent with the dual role of IL-1 $\beta$  reported, where it can both facilitate cell survival, the transient response, or enter a state of chronic inflammation, the locked state<sup>14,17</sup>. Notably, the islets display at least one NF- $\kappa$ B/IL-1 $\beta$  pulse in response to a stimulus, and therefore, even the islets that eventually lock also display an initial transient IL-1 $\beta$  response (Fig. 2A, B), suggesting that the chronic inflammation state will always follow after the initial acute phase with transient IL-1 $\beta$ .

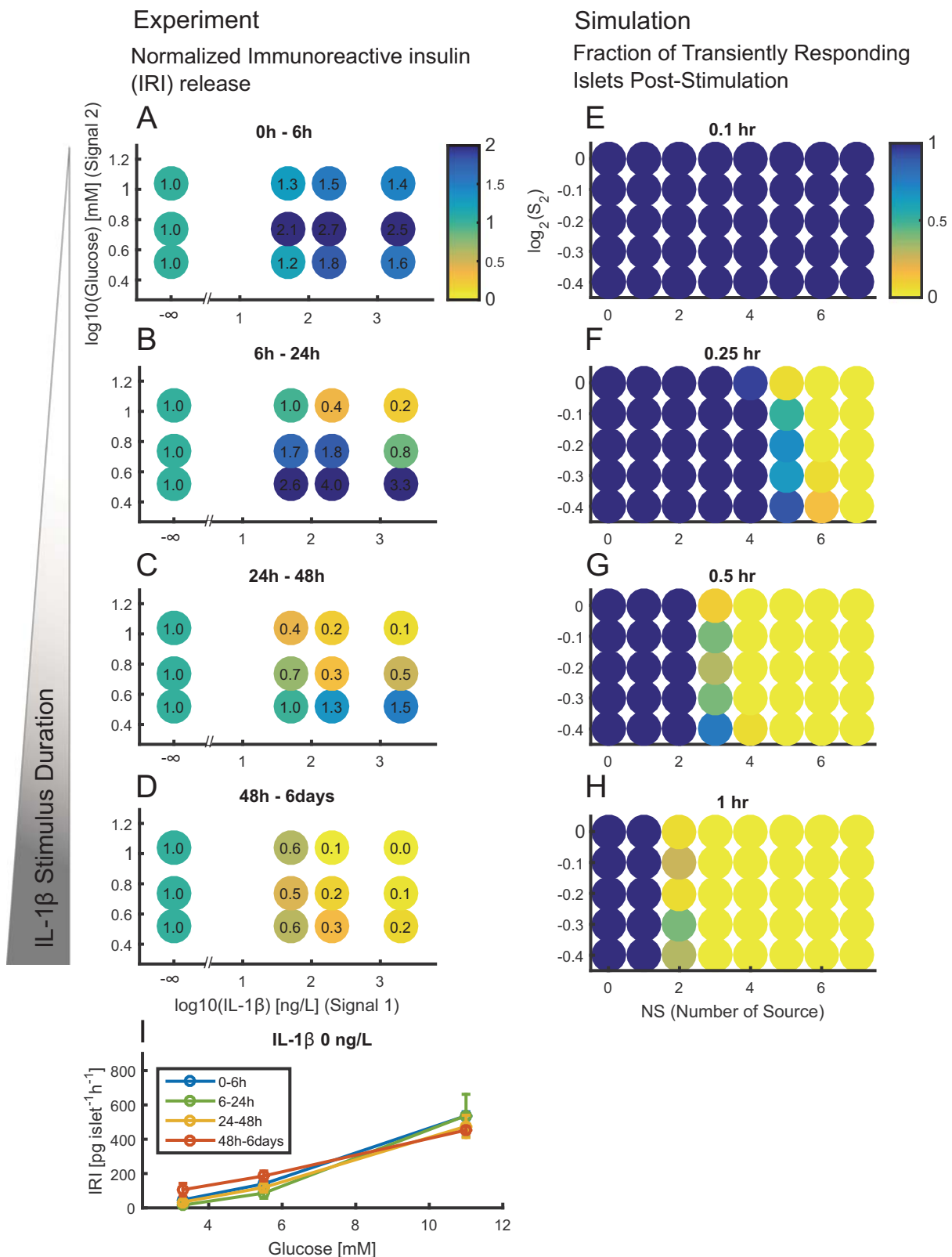
Having established two distinct modes of IL-1 $\beta$  response, we investigated if the transition between the two modes is gradual, with, e.g., islets gradually increasing production levels of IL-1 $\beta$  with increasing  $S_{I,2}$  or sudden, with a discontinuous jump from low to high IL-1 $\beta$ .

We found that the transition is sharp (Fig. 2C, D and confirmed by the larger parameter scan shown in Fig. 3E–H): a small increase in either Signal 1 or Signal 2 (or both) can have a drastic effect on the probability of locking. Notably, close to the transition, locked and non-locked islets can coexist: despite being exposed to the same values of  $S_I$ ,  $n_s$  and  $S_2$ , some islets lock into a state with sustained level of IL-1 $\beta$ , whereas others show transient behavior. In this “co-existence regime,” the fate of an individual islet is determined by the exact geometrical positioning (and timing) of the  $S_I$  sources. This finding is in line with the current knowledge that in the same pancreas there can be co-existing subpopulations of inflamed and non-inflamed islets<sup>15</sup> (measured by number of infiltrating macrophages).

**The model recapitulates the fact that glucose narrows the time window in which IL-1 has beneficial effects**

Having established the emergence of transient and persistent modes of IL-1 production within the single islet, we wanted to further test if our model is consistent with the experimental observation that the time window of the beneficial effect from IL-1 is shorter at higher glucose levels (corresponding to higher  $S_2$ )<sup>37</sup>.

As mentioned in the “Introduction”, the beneficial effect of transient IL-1 exposure is manifested by increased insulin release. However, long exposure to high levels of IL-1 leads to cell death and decreased insulin production within the islet. Therefore, the ability of the islet to produce insulin can be used as a proxy of its state. For simplicity, we assume that the in silico islet locked in a persistently elevated IL-1 state is representative of the real islets where IL-1 exposure has deleterious effects, i.e., those with decreased insulin release.



Palmer et al.<sup>37</sup> measured the immunoreactive insulin (IRI) release in islets that had been exposed to different glucose concentrations (3.3, 5.5 and 11 mM) for different durations of time (6, 24, and 48 h and 6 days of culture). As insulin release increases with increasing glucose concentrations in the absence of IL-1 $\beta$  (Fig. 3I), to extract the effects of IL-1, one has to normalize for these baseline IRI releases. To test the complex dual effects of

IL-1 $\beta$  on  $\beta$ -cell function different concentrations of IL-1 $\beta$  (50, 500, and 2000 ng/L) was added to the culture, and IRI release was measured. To focus on the effects of IL-1 $\beta$ , we have plotted the values reported in ref. 37 in Fig. 3A–D, where we normalized IRI release at each glucose and IL-1 $\beta$  level by the corresponding values in the absence of IL-1 $\beta$  (Fig. 3I). Qualitatively, the effects of IL-1 are glucose-independent at brief (0–6 h, Fig. 3A) and long

**Fig. 3 | Transition from IL-1 protective to deleterious effects is accelerated under higher  $S_2$ .** **A–D** Experimental data for the time course of the Immunoreactive Insulin Release (IRIR) normalized with respect to IRIR in absence of IL-1 $\beta$  based on data from ref. 37. Color codes for the fold change in IRIR in presence of the IL-1 relative to the IRIR in absence of IL-1. The doses of IL-1 (corresponding to  $S_1$ ) are specified on the x-axis, and glucose (corresponding to Signal 2,  $S_2$ ) levels on the y-axis. **A** Islets were exposed to the specified glucose and IL-1 levels for 6 h, and the color indicates measured normalized IRIR over the period 0–6 h. **B** Similar to (A), but cumulative IRIR was measured for the period of 6–24 h. **C** Similar to (A), but cumulative IRIR was measured for the period of 24–48 h. **D** Similar to (A), but cumulative IRIR was measured for the period of 48 h–6 days. **E–H** Simulation results showing the fraction of simulated islets responding transiently at a given value of Signal 1 dose,  $S_1 \times NS$  (x-axis) and  $S_2$  (y-axis). The fractions are color-coded from yellow corresponding to 0, and thus no islets in transient state (i.e., all are locked) to blue corresponding to 1 (all islets responding transiently). The fraction for each circled point is calculated based on 20 simulations of individual islets (similar to Fig. 2A) of a radius of 6.7 cells with randomly placed  $S_1$  sources within the islet. Similar to the experiments, the probability of transitioning to the “locked state” increases as function of external  $S_1$  stimulus, inflammasome activation ( $S_2$ ) and the duration of external  $S_1$  stimulus. Each external source has an  $S_1$ -value of  $25 \text{ h}^{-1}$  and  $p = 1400 \text{ h}^{-1}$ , NS is a number of sources.

(2–6 days, Fig. 3D) exposures. At all glucose levels, brief exposure to IL-1 increases, and long exposure to IL-1 inhibits insulin release. The switch between the two modes, which happens at intermediate IL-1 durations, is however glucose-dependent, occurring already after 6 h at the highest glucose concentration (Fig. 3B).

For our model to be consistent with these results, *brief exposure* to  $S_1$  should result in a majority of islets in transient mode, which is indeed the case (Fig. 3E, F). On the other hand, experiments showed that long exposures to IL-1 $\beta$  (48 h–6 days) lead to decreased IRI release when compared to the reference values (Fig. 3D). This is also consistent with our model outcomes for the situation where the  $S_1$  sources are turned on for an increased period of time (1 h, Fig. 3H). In this case, the model predicts increased probabilities of islets locking into the persistent mode, which we interpret as being related to impaired insulin response. We note that the exact timing of the model does not match the longer time period investigated in the experiments.

At the intermediate durations (6–24 and 24–48 h), experiments show that switching from the transient to the persistent mode should happen first where  $S_2$  is highest (Fig. 3B, C). We find that this is indeed the case (Fig. 3E–H). Notably, the islets exposed to IL-1 $\beta$  for a longer time display an increasingly impaired response to glucose stimulation. This is consistent with our simulations, where the parameter range of  $ns$ ,  $S_1$  and  $S_2$  that leads to locked islets increases with longer exposure to  $S_1$ .

To our knowledge, it is not known why the switching from insulin-enhancing to insulin-inhibiting modes happens earlier at higher glucose concentrations. While it has been shown that glucose potentiates IL-1 $\beta$ -induced nitric oxide production—one mediator of the IL-1 $\beta$  cytotoxic effect—the time dependence has not been addressed<sup>38</sup>. Our results suggest that the time dependence may come as a result of the modulation of the positive feedback loop by  $S_2$ , in that stronger positive feedback accelerates the transition to “locked” state and thus to insulin-inhibiting mode of IL-1 $\beta$ . When we compare simulation and experimental results, the region of parameters where we find locked islets increases much faster in simulations than the corresponding region for the islets with impaired Immunoreactive Insulin Release (IRI) release in the experiments, Fig. 3. In the experimental settings, inflammasome activation (Signal 2) is likely to increase gradually over time, since the islets are exposed to the combined stress of high glucose and IL-1 $\beta$ . This is not explicitly incorporated in our model;  $S_2$  is set to a certain constant value at the beginning of our simulations but could be made a function of exposure time to fit the experimental transitions.

### The effect of IL-1 receptor antagonist on islet fate

Because IL-1 $\beta$  is an established part of T2D pathogenesis, different types of treatments targeting the cytokine have previously been investigated. Clinical studies with anakinra, a recombinant IL-1 receptor antagonist (IL-1Ra) have showed improvements in glycemia and  $\beta$ -cell function<sup>22</sup>. Remarkably, a 3-month anakinra treatment had a durable effect, lasting for over 39 weeks after anakinra withdrawal. Other studies targeted the increased level of cytokines through IL-1 $\beta$  antibodies, with a similar improvement of  $\beta$ -cell function and lowered inflammation<sup>39,40</sup>. While the mechanism behind the persistent effects after drug withdrawal is unknown, it has been hypothesized that it could result from interrupting the auto-inflammatory positive

concentrations of glucose and IL-1 $\beta$ . The islets were exposed to increasing durations of IL-1 $\beta$  from (A) to (D). **E–H** Simulation results showing the fraction of simulated islets responding transiently at a given value of Signal 1 dose,  $S_1 \times NS$  (x-axis) and  $S_2$  (y-axis). The fractions are color-coded from yellow corresponding to 0, and thus no islets in transient state (i.e., all are locked) to blue corresponding to 1 (all islets responding transiently). The fraction for each circled point is calculated based on 20 simulations of individual islets (similar to Fig. 2A) of a radius of 6.7 cells with randomly placed  $S_1$  sources within the islet. Similar to the experiments, the probability of transitioning to the “locked state” increases as function of external  $S_1$  stimulus, inflammasome activation ( $S_2$ ) and the duration of external  $S_1$  stimulus. Each external source has an  $S_1$ -value of  $25 \text{ h}^{-1}$  and  $p = 1400 \text{ h}^{-1}$ , NS is a number of sources.

feedback loops<sup>41</sup>. We set out to test this hypothesis with our model. The result of blocking IL-receptors with the antagonist effectively corresponds to increasing the activation threshold of NF- $\kappa$ B in the model. This can be done in two ways: preventive treatment, where the drug is given before islets have transitioned into the locked state or reactive treatment, where the drug is given after the islets transitioned into the locked state.

We find that preventive treatment offsets the transition by shifting the locked state to higher  $S_2$ , Fig. 4A. In other words, islets can withstand higher levels of glycemia or free fatty acids in the presence of the antagonist. To assess the degree of dose-dependency of the simulated treatment, we have normalized the results in Fig. 4A by the untreated results (corresponding to  $1.0 K_1$ ), see Fig. 4C. The normalized values can be thought of as islets “rescued” by the treatment. We find that the effect is dose-dependent in several ways: first, within a certain range of  $S_2$  ( $\log_2 S_2 = -0.92$ – $-0.9$ ), the fraction of “rescued” islets increases with increasing dose. Second, the range of  $S_2$  where the treatment has an effect also increases with the dose. While the trend is the same for the case of reactive treatment, where antagonist is added after islets have already locked, we find that reactive treatment is less efficient. Rescue of about 50% of the islets required 10-fold higher doses (higher activation threshold) compared with the preventive treatment.

While interfering with the positive feedback loop through both preventive and reactive treatments can rescue the islets from locking, we find that removing the treatment (resetting the  $K_1$  back to pre-treated values) would not have long-lasting effects as long as  $S_1$  and  $S_2$  are unchanged. It is however known that the IL-1R antagonists improve glycemia and FFA levels in T2D patients<sup>41</sup>. This corresponds to lowering  $S_2$  prior to treatment withdrawal in our model, and, in this case, the effect of single islet unlocking with IL-1RA would be long-lasting.

### Islet shape, size and internal geometry play crucial roles in the fate of islets

Human islets are diverse in size and geometrical arrangement of  $\beta$ -cells. Small islets tend to have a core-mantle-shaped structure with a homogenous core of  $\beta$ -cells, surrounded by  $\alpha$ - and  $\delta$  cells. Larger islets are more complex, as the core-mantle geometry is replaced by a heterogeneous mixture of  $\alpha$ -,  $\beta$ - and  $\delta$  cells and fenestrated capillaries<sup>24</sup>. Notably, it is large islets that are the first to be lost in T2D patients<sup>24</sup>. While the mechanism is currently unknown, there is strong evidence that inflammation plays an important role. First, Ehses et al.<sup>15</sup> found that in murine models of T2D, macrophages infiltrate large islets first. Second, Youm et al.<sup>25</sup> showed that ablation of NLRP3 inflammasome in chronically obese mice protected large islets from inflammation-induced death.

These observations, together with our findings, suggest that the larger islets may have a higher propensity to lock and, as a consequence, would be compromised at lower levels of  $S_2$ . In order to test this, we first varied the size of the core-mantle-shaped islets and monitored the fraction of persistently responding islets with increasing  $S_2$  as described in Fig. 2D. We found that the transition from transient to persistent IL-1 response indeed occurs at lower values  $S_2$  when islets are larger (Fig. 5A).

To further quantify how the transition depends on the shape of the islet, we have implemented an experimentally reported configuration from ref. 18 (Fig. 5B, left). Despite a relatively large number of cells (159 cells), this

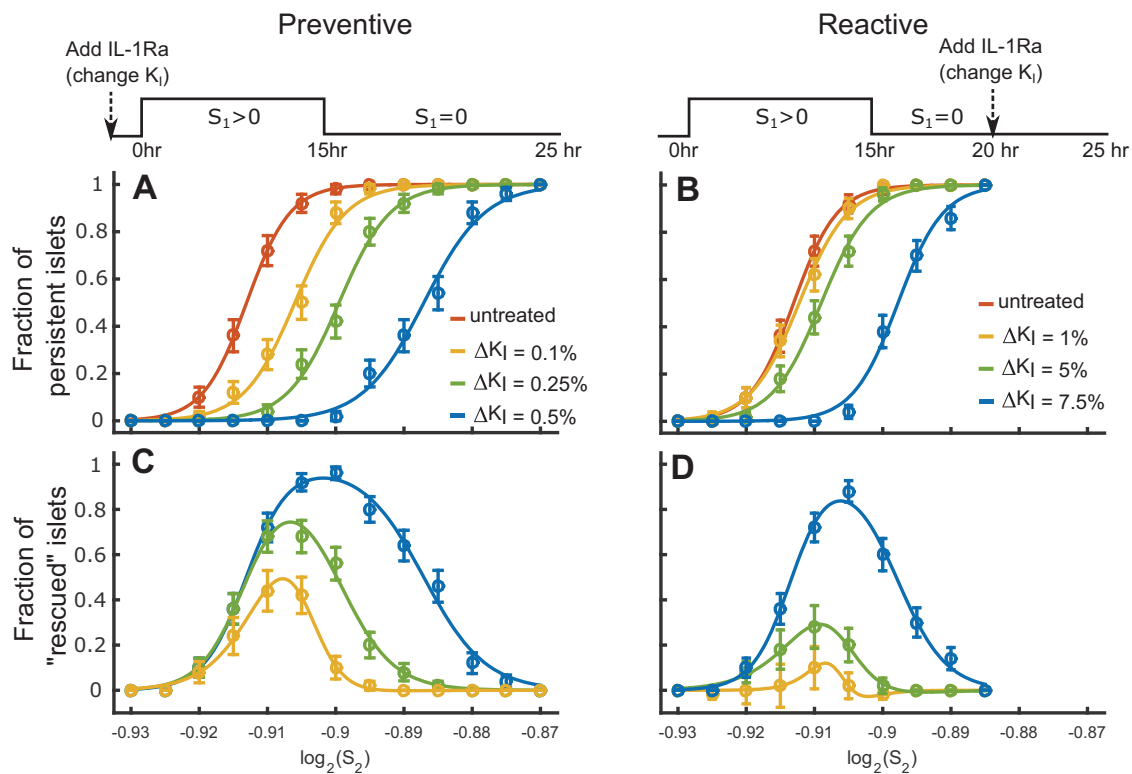


**Fig. 4 | Simulated effect of preventive and reactive treatment with IL-1β antagonists.** **A** The transition of islets from transient to persistent inflammation with increasing levels of  $S_2$ . Preventive treatment is simulated by changing the activation threshold,  $K_1$ , prior to  $S_1$  exposure. Increasing  $K_1$  offsets  $EC_{50}$  to higher  $S_2$ . Simulations of the untreated case ( $1K_1$ , red).  $K_1$  is increased by  $\Delta K_1$  0.1% (yellow), 0.25% (green) and 0.5% (blue). **B** Reactive treatment is simulated by changing activation threshold after  $S_1$  exposure. The results of the simulations in the untreated

case with ( $1K_1$ , red) and increased activation threshold by 1% (yellow), 5% (green) and 7.5% (blue). **C, D** The fraction of “rescued” islets represented by the relative change (treatment – no treatment) in fraction of locked islets. The reactive treatment has a weaker effect than preventive treatment, and the range of  $S_2$  where the treatment has the maximum effect is dose-dependent. To identify  $EC_{50}$ , all data was fitted by sigmoidal curves (colored lines), see “Methods”. Results are from simulations in islets of radius 6.7 cells.

configuration is more robust and can sustain higher levels of  $S_2$  ( $\log_2(S_2^{lock}) = 0.75$ ) without locking compared to smaller islets with core-mantle configuration (127 cells,  $\log_2(S_2^{lock}) = 0$ ). Consistent with this result, islets with ISCs distributed in a donut-shape, transit to the locked state at even higher  $S_2$ . The results are qualitatively the same, if we fix levels of  $S_2$  and increase  $S_1$ , Fig. 5C. If we assume both signals are constant throughout the pancreas, larger islets would be at higher risk of entering a self-sustained inflammatory response, simply because the critical  $S_2$  level is lower, consistent with observations in T2D patients and murine models<sup>24</sup>. In our simulations, a greater mixture of endocrine cell types or capillaries that can act as sinks can contain this threat.

For each islet shape, there is a parameter range where transiently and persistently responding islets coexist. This is not the result of  $S_1$  and  $S_2$  but rather the internal geometry of sources in the islet. The position of the external sources is random and is the only source of stochasticity in our simulations. Interestingly, the region of co-existence is much broader for the human- and donut-shaped islet, indicating that the position of external sources within these islet types has a greater impact on islet fate. Voids, corresponding to non-ISCs or capillaries, could be a factor that increases fate diversity since a central sink can create a delay in the excitation between ISCs at different ends of the islet. In compact islets, the excitation will spread more or less uniformly, because we use a high diffusion constant compared with islet size.

To investigate why there is a co-existence of modes, we have quantified if some positions of  $S_1$  are more likely to induce persistent modes while others are transient. In Fig. 5D, we show the frequency of source positions in transient and persistent modes. We find that the local density of ISCs around the sources is higher in persistent compared to transient modes. This is quantified in the box plot of Fig. 5E, where there are significant differences

in the average number of ISC neighbors within the diffusion length,  $\lambda = \sqrt{D\tau_I}$ , between islets of different fates. Hence an inflammatory response located at the center of an islet is more critical than peripheral cell defects or a response close to capillaries, where the cytokines can be cleared from the islet.

### Robustness of the results to parameter choices and cell-to-cell heterogeneity

In order to test the robustness of the model, we conducted a parameter sensitivity analysis.

As described above, the parameters  $k_{IN}$ ,  $k_{RN}$ ,  $k_{NR}$ , and  $\tau_R$ , have been hand-fitted to simulate a simplified model for transient activation of NF-κB with a peak around 2 h<sup>34</sup>. We focused on less constrained parameters related to the production, degradation and diffusion of IL-1β (Fig. S6). As the transition from transient to persistent inflammation in islets is one of the key results, we have used it as a main readout for assessing how sensitive the model outcomes are to parameter changes. For a given parameter set and given number of  $S_1$  sources (ns), we simulate islet response to transient exposure to  $S_1$  signal. We use levels of IL-1β after  $S_1$  signal has been removed as a marker for the islet being in a locked (persistently elevated) or unlocked (returning to pre-stimulated level) state.

To systematically quantify the transition point, we have fitted the outcomes of such an  $S_1$ -scan to a step-like sigmoidal function  $f(x) = V_{max} \frac{(x/K)^{10}}{1+(x/K)^{10}}$ . The fitted  $V_{max}$  and  $K$ , represent the *levels of the IL-1 in locked islets* and the *transition point* (number of  $S_1$  sources at which islet transitions to a locked state), respectively.

We found that for the tested perturbations, the model still recapitulates the characteristic transition from transient (unlocked) to

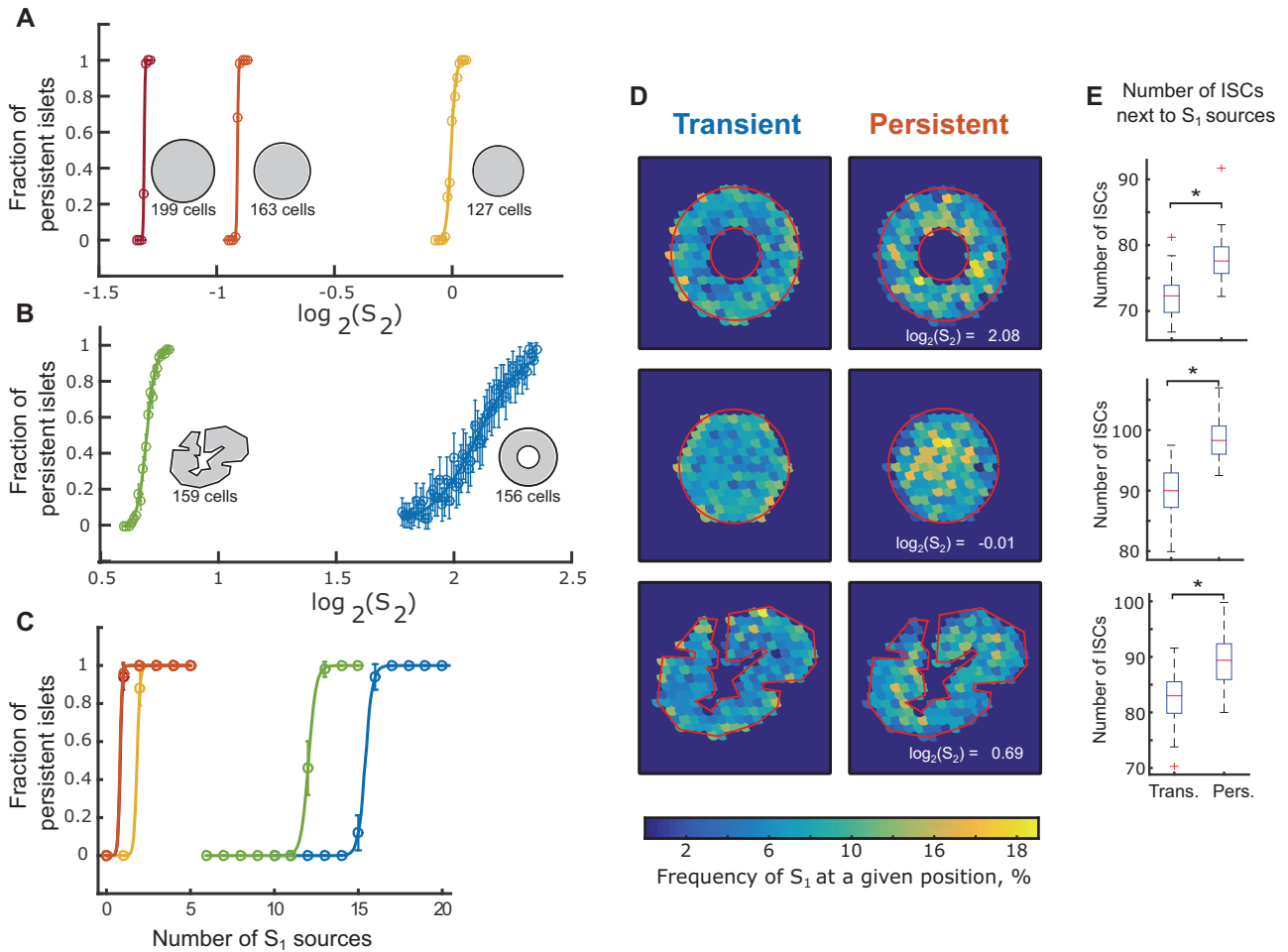


**Fig. 5 | Islet size and shape influence its propensity to lock.** **A** Larger islets transition to the persistent mode at lower  $S_2$ . The fractions of persistent islets (simulation results) are color-coded according to the islet sizes, red, orange and yellow corresponding to islets consisting of 199, 163 and 127 cells. **B** Islets with few or no ISCs in the core sustain high values of  $S_2$  without locking. Here green and blue mark the simulated fractions of persistent islets for respectively “human” and a donut-shaped islets. The islet to the left is a cross-section of a human islet configuration experimentally reported in ref. 18. The results are shown for  $S_1 = 25 \text{ h}^{-1}$  at each source, with number of  $S_1$  sources  $n_s = 10$ . **C** Large core-mantled shaped islets are also more prone to locking when exposed to increasing  $S_1$ .  $S_1$  at each source is  $25 \text{ h}^{-1}$ ,  $\log_2(S_2) = 0.5$ . The color correspond to the islet sizes and configurations as defined in **A** and **B**.

**D** The sources of  $S_1$  positioned deep in the bulk of the ISCs increase islet propensity to lock. The frequency of  $S_1$  at a given position is color-coded in islets that either respond transiently (left) or persistently (right). Results are sampled over 200 simulations where the position of 10 sources of  $S_1$  was chosen randomly among ISCs while other parameters were kept constant ( $S_1 = 25 \text{ h}^{-1}$ ). **E** The density of ISCs in the vicinity of  $S_1$  sources is estimated by the average number of ISCs within diffusion length  $\lambda = \sqrt{D\tau_1}$  from  $S_1$ . For all shapes, the number of ISCs next to  $S_1$  sources is significantly smaller in transiently responding islets. (Kolmogorov-Smirnov test, comparing the distributions for each islet fate, see “Methods”). All simulations were run with  $p = 1400$ .

persistently elevated (locked) IL-1 $\beta$  levels in single islets and that the probability of “locking” increases with increasing level of Signal 1. In regards to sensitivity, parameters fall into two categories, the less sensitive  $\tau_I$ ,  $\tau_I$ , and  $D$  and one sensitive parameter,  $p$ . The less sensitive are the ones related to degradation and diffusion of IL-1 (different values of the parameters  $\tau_I$ ,  $\tau_I$ , and  $D$ ). The variations in the transition point,  $K$ , do not seem to be sensitive to the exact values of these parameters (Fig. S6) but appear to be primarily dominated by the exact positioning of  $S_1$  sources. On the other hand, increasing  $p$ -values (describing the NF- $\kappa$ B mediated production of de novo IL-1 and effectively corresponding to the strength of the IL-1 positive feedback) correlated with increasing probability of locking (Fig. S6D). This is in line with our earlier findings<sup>27,29</sup>, where the strength of the positive feedback was identified as a bifurcation parameter. Extreme values of  $p$  lead to a disappearance of the co-existence regime: when  $p$  is small enough, no islets will lock, and when  $p$  is high enough, all islets will lock for the entire range of Signal 1 dose that was investigated. The level of IL-1 in the sustained state,  $V_{\max}$ , also increases with increasing  $p$ -values (Fig. S6E).

The diffusion constant used in the main results was based on the estimate of diffusion of IL-1 $\beta$  from its molecular weight in cell-free medium; however, binding of IL-1 in the extracellular matrix is likely to result in a lower effective diffusion<sup>42</sup>. We accounted for this by checking that our results do not change qualitatively if the diffusion constant is further decreased up to 100-fold, see Supplementary Movies 7–9. Lowering the diffusion constant shifts and decreases the relevant parameter regimes ( $S_1$ ,  $S_2$  and  $p$ ), since less cytokine is removed from the islets. This scenario can lead to interesting phenomena, as seen in excitable media, such as traveling waves or spiral patterns. In rare instances, source position can generate waves that travel around central arteries (see Supplementary Movies 10 and 11).

Islets of Langerhans are subject to cell heterogeneity—not only in different cell types but also variations in protein levels inside and outside the cells. Noise in parameters such as inflammasome activation or clearance of inhibitor can have a large impact on the local dynamics, and we have therefore tested that the main results of our model are also valid when we introduce cell-to-cell heterogeneity in model parameters. In practice, we introduce such cell heterogeneity by modeling different parametrizations in

each cell by drawing individual values of the parameters from a normal distribution with a mean given by the reference parameters set (Table 1 in “Methods”) and a width given by the coefficient of variation, CV. We choose random values for the parameters  $\tau_I$ ,  $\tau_T$ ,  $p$ , and the activation threshold  $K_I$  (reference value is equal to one, as we model the rescaled equations, Fig. 1C, also see “Methods” section). We do not choose random values for the diffusion constant, since this is inherently a global variable. Notice also that we have not performed a parameter scan of the activation threshold, since the model is scaled according to this parameter. It is however relevant to investigate cell-to-cell variation in the activation threshold, as studies have shown that cells do exhibit variations

The results of simulations including cell-to-cell variability are shown in Supplementary Fig. S7. We found that the model still predicts transient and persistent production of IL-1 $\beta$  and that the co-existence regime widens when cell-to-cell heterogeneity is introduced (Supplementary Fig. S7C–E).

## Discussion

We investigated the possible dynamical modes that can be generated by the IL-1 regulatory network in pancreatic islets in response to pro-inflammatory,  $S_1$ , and metabolic,  $S_2$ , cues. Notably, we find that there are only two—*transient* and *persistent*—dynamical modes. Weak cues result in *transient* upregulation of IL-1, while strong cues push the system into a state where IL-1 is *persistently* upregulated, even when the initial cues are removed. These modes are encoded by the fast positive IL-1 feedback and slow negative feedback on NF- $\kappa$ B. Islets respond transiently, when the strengths of these feedbacks are balanced, and persistently, when positive feedback is dominating. When the negative feedback is dominating, the response will be diminished or completely ablated. The progression of T2D can be seen as imbalanced feedback, whereas beneficial effects of antagonists, including IL-1R antagonists<sup>41</sup> to pro-inflammatory cytokines and chemokines, can be thought of as a tool to restore the balance (see Fig. 6).

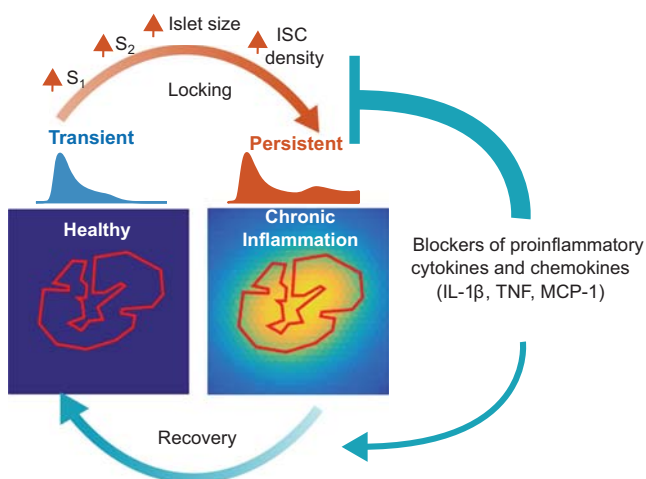


**Fig. 6 | Summary of the results and model predictions.** The combination of the negative and positive feedback regulating the NF- $\kappa$ B response results in two qualitatively different islet fates. When briefly exposed to pro-inflammatory stimuli, some islets will upregulate IL-1 $\beta$  transiently while others persistently. The increase in the pro-inflammatory ( $S_1$ ) or metabolic ( $S_2$ ) cues, size of the islets or density of IL-1-secreting cells increases the likelihood for the islet to respond persistently. Blockers of pro-inflammatory cytokines and chemokines weaken the positive feedback loop and offset the transition into persistent mode (flat-headed arrow). Higher doses can reverse the transition; however, concomitant reduction in  $S_2$  is required for the long-term effect upon treatment withdrawal.

## Offsetting and reversing the transition by IL-1 receptor antagonists

While it is often mentioned that the beneficial effect of IL-1 antagonism is derived from “*interruption of vicious cycles of auto-inflammatory induction*,”<sup>41</sup> our results introduce a note of caution against complete interruption of the local auto-inflammatory positive feedback, as it is likely to be essential to mount a protective transient response. Instead of “*interrupting*” the IL-1 positive feedback, the aim should rather be at “*restoring*” the balance between the two feedbacks (which is likely what happens at the administered doses of IL-1 antagonists). We modeled this effect by weakening the positive feedback, but an alternative way of restoring the balance would be to strengthen negative feedback. In that respect, the recent results with lysine deacetylase inhibitor Givinostat<sup>43</sup> pose an interesting question of how hyperacetylation of the p65 subunit, a component in the pathway that should affect the strengths of both feedbacks, alters the balance between them.

Our simulations with IL-1Ra suggest that disrupting the auto-inflammatory positive feedback *at the single islet level* is necessary, but not sufficient to explain the observed long-term improvement in T2D patients. It can however explain the long-lasting effect when combined with a decrease in inflammasome activity, the  $S_2$ -value. In single islets, this decrease may happen either locally, for example, through the pathway of pro-inflammatory cytokines  $\rightarrow$  ER-stress  $\rightarrow$  inflammasome<sup>3,44,45</sup> or through a global, systemic effect, where improved  $\beta$ -cell function leads to normalized glycemia and decrease in inflammasome activity.

Our results are thus consistent with the recent *in silico* models of the therapeutic effect of IL-1Ra focusing on whole-body effects by Zhao et al.<sup>46</sup> and Palmer et al.<sup>47</sup>. Both models implement the dual effect of IL-1 $\beta$  on proliferation and apoptosis and predict how treatment affects  $\beta$ -cell mass. In an extensive disease progression model, Palmer et al. are able to reproduce sustained improvements in insulin secretion after a *transient treatment* with IL-1Ra and conclude that this is mainly due to an improvement in  $\beta$ -cell function rather than  $\beta$ -cell mass<sup>47</sup>. In line with this, Zhao et al. find that treatment with IL-1Ra *must be transient* to see disease improvement as the treatment also inhibits the proliferation of  $\beta$ -cells. This may explain why IL-1Ra or IL-1 $\beta$  antibody therapy for 9–12 months failed to improve beta-cell function in T1D patients<sup>32</sup>.

It is tempting to consider that IL-1Ra may be yet another component of the “*combined*” slow negative feedback of the IL-1 $\beta$  $\rightarrow$ IKK $\rightarrow$ NF- $\kappa$ B pathway. There are NF- $\kappa$ B binding sites upstream of the IL-1Ra promoter<sup>48</sup>; IL-1Ra is reported to be upregulated by IL-1 $\beta$  in endometrial stromal cells<sup>49</sup>; the expression of IL1Ra follows the expression of IL-1 $\beta$  when induced by LPS in Schwann cells<sup>50</sup>, and both are upregulated in response to leptin<sup>51</sup> in  $\beta$ -cells. Thus, as is the case with our combined negative regulator, R, IL-1Ra may be upregulated transiently because of transient IL-1 $\beta$  activation when the positive and negative feedbacks are balanced.

## Large and dense islets are more likely to transit into persistent mode

Our model predicts that in the population of islets exposed to the same conditions, both transiently and persistently responding islets will be observed. This co-existence is a result of geometrical differences in islet structures or in spatial configurations of initial pro-inflammatory cues.

*Large and dense* islets, where many of the ISCs are next to each other, are more likely to transit into the *persistent* mode. Due to extracellular diffusion, ISCs surrounded by non-ISC are exposed to lower IL-1 than the cumulative IL-1 secreted by several neighboring ISCs. Thus, effectively higher density of ISCs corresponds to a stronger positive feedback experienced by individual cells. Therefore, large and dense islets will be biased to respond persistently. Notably, Striegel et al.<sup>52</sup> found that  $\beta$ -cells are more proximal to each other in islets of T2D patients, which suggests that assuming all the other parameters equal, islets of T2D patients are more likely to transit into persistent modes.

These results may unify the experimental observations by Ehse et al.<sup>15</sup> and Youm et al.<sup>25</sup> and provide an explanation to a hitherto unanswered

question of how the size of the islets may relate to their inflammatory state and eventual death in T2D<sup>24</sup>. They also may suggest an evolutionary perspective on limiting the size of the islets by distribution into  $1 \times 10^6$  separate micro-organs dispersed in the exocrine pancreas: While it has been proposed that the size of the islets may be optimized for synchronization in  $Ca^{2+}$  bursts and glucose-induced insulin release<sup>53</sup>, our results suggest that clustering  $\beta$ -cells in physically separated small islets may serve an additional purpose of reducing inflammation and isolating it to single islets.

The coupled fast positive and slow negative feedbacks classify IL-1 $\beta$  regulation as excitable media phenomena<sup>29</sup>. It is well established that information processing or “chemical computing” can be performed by certain spatial configurations of excitable and non-excitable units<sup>54</sup>. Our results, showing that the transition from protective (transient) to deleterious (persistent) modes strongly depends on islet size and the geometrical configurations of excitable ISCs, open an exciting possibility that the spatial organization of the islets may reflect “cytokine computing” at the islet level.

### Outlook and suggestions for experimental validations

Our results call for quantitative experiments at the single islet level. While technically challenging, it now becomes conceivable to sample cytokine secreted by single islets using microfluidic devices<sup>55</sup>. However, antibody staining and RNA FISH to detect levels of IL-1 protein and mRNA in single pancreatic islets can also validate a number of our predictions. Our model will be validated if, with increasing doses of the cues, there will be two subpopulations of islets, one responding transiently and another persistently, and with a bias towards larger islets in the persistent fraction.

Our approach and results are likely to apply beyond IL-1 $\beta$  in pancreatic islets, for example, to other pro-inflammatory cytokines (e.g., TNF, IL-6, MCP-1), where it is known that both positive and negative feedbacks are at the core of the regulation.

Thus, the complexity of the model and the assumptions required, such as uniform cell distribution and fixed diffusion rates, may limit its applicability in a real-life biological setting. Exploring the interactions between multiple cytokines and extending the model to include recent findings on cellular heterogeneity within islets<sup>56–58</sup> should provide deeper insights into the islet inflammatory processes in diabetes. Thus, further experimental validation in actual islet samples will be crucial to verify the model predictions and enhance its utility in clinical applications.

## Methods

### Model setup and variable rescaling

The model used in this work is based on the three-variable NF- $\kappa$ B model by Yde et al.<sup>27,29</sup>. We modified the model to increase similarity with the system of pancreatic  $\beta$ -cells, i.e., introducing pro-IL-1 $\beta$  and IL-1 $\beta$ . The fourth variable, pro-IL-1 $\beta$ , was included since glucose affects IL-1 $\beta$  secretion through inflammasome and caspase-1 activation, which cleaves pro-IL-1 $\beta$  into mature IL-1 $\beta$ <sup>59</sup>. This introduces a new dynamical behavior compared with the old system, since a low signal 2 can lead to a build-up of pro-IL-1 $\beta$ , which was not possible in the old model. In the regime of high signal 2, the translation rate of pro-IL-1 $\beta$ ,  $p$ , can be a limiting factor.

The model takes the following form before rescaling:

$$\frac{dn}{dt} = k_{IN} \frac{i^2}{i^2 + K_I^2} (N_{tot} - n) - k_{RN}r \tag{5}$$

$$\frac{dr}{dt} = k_{NR}n - \frac{r}{\tau_R} \tag{6}$$

$$\frac{di'}{dt} = Pn - \left( S_2 + \frac{1}{\tau_I} \right) i' \tag{7}$$

$$\frac{di}{dt} = s_1 + S_2 i' - \frac{i}{\tau_I} + D\nabla^2 i \tag{8}$$

$n$  is the nuclear NF- $\kappa$ B,  $r$  is an effective inhibitor of NF- $\kappa$ B,  $i'$  is pro-IL-1 $\beta$  and  $i$  is mature IL-1 $\beta$ . The inactive NF- $\kappa$ B, ( $N_{tot} - n$ ), is resident in the cytoplasm but can be activated by IL-1 $\beta$  binding to surface receptors. A Hill-term describes the receptor binding and transportation of NF- $\kappa$ B into the nucleus. The Hill-term, which is non-linear, is the source of bi-stable behavior in the system. NF- $\kappa$ B upregulates both  $i'$  and  $r$  linearly and dependent on the  $S_2$  parameter,  $i'$  is transformed into  $i$  which can diffuse between cells in an auto- and paracrine manner. For simplicity, the model assumes the degradation of  $r$ ,  $i'$  and  $i$  is linear as expected by dilution. Active degradation is normally described by Michaelis-Menten kinetics but reduces to a linear term in the saturated regime. For simplicity, the inactivation of  $n$  by  $r$  is modeled as a linear term, but should be modeled by Michaelis-Menten kinetics. Because  $r$  represents several inhibition factors that work at different time scales, the model does not describe secondary oscillations normally expected by NF- $\kappa$ B. The focus of this model is the transient behavior in response to the initial and sustained stimulus and transitions between qualitative types of response after the initial stimulus is removed.

We rescaled the model to eliminate a few parameters.  $n$  and  $r$  are rescaled in terms of  $N_{tot}$ .  $i$  and  $i'$  are normalized with respect to the activation threshold  $K_I$ . The parameter  $P$  is rescaled by  $N_{tot}/K_I$  and  $s_1$  is rescaled by  $K_I$ . The rescaled variables and parameters are given by:

$$N = n/N_{tot}$$

$$R = r/N_{tot}$$

$$I' = i'/K_I$$

$$I = i/K_I$$

$$p = PN_{tot}/K_I$$

$$S_1 = s_1/K_I$$

The rescaled equations are shown in the main article.

### Model parameters

We hand-fitted  $k_{IN}$ ,  $k_{RN}$ ,  $k_{NR}$  and  $\tau_R$  to fit the time scale of the first peak in NF- $\kappa$ B oscillations<sup>33</sup>. For this fitting, we consider only equations for  $N$  and  $R$ , and cytokine dynamics was ignored, by substituting the sigmoidal term  $\frac{I^2}{I^2 + K_I^2}$  with a step function going from zero, in the absence of NF- $\kappa$ B stimulus, to 1 when stimulated.

The timing of the first peak in the model has a small delay and is a bit wider than the peak of actual NF- $\kappa$ B oscillations. This is because several inhibitors are collapsed into the  $R$ -variable, which also removes the secondary NF- $\kappa$ B oscillations normally observed<sup>27,29</sup>.

The diffusion constant is in units of cell size. We used a cell size of  $15 \mu\text{m}$ <sup>18</sup> and  $D = 900 \mu\text{m}^2/\text{min}$ <sup>31</sup> the diffusion on a grid of cells is  $D \approx 300 \text{ cells}^2/\text{h}$ . Note, IL-1 $\beta$  has been shown to be released by Gasdermin pore formation<sup>60</sup>. We have not modeled the export step explicitly, but it can introduce a further delay between NF- $\kappa$ B activation and mature extracellular IL-1 $\beta$ .

### Numerical integration

The ordinary differential Eqs. (1)–(4) were solved numerically in C++ and the analysis done in Matlab. The simulations for the cell-cell variability and parameter sensitivity analyses (Supplementary Figs. S6 and S7) were performed in Python. We organized the cells on a hexagonal grid to have equal distance to nearest neighbors. Each IL-1-producing cell was programmed as an object with local concentrations of  $N$ ,  $R$  and  $I'$  and the total size of the 2D system was 75 by 75 cells. All simulations included only a single islet, placed in the middle of the hexagonal grid. The islet was simulated using a certain radius  $R$  around the center of the grid (in Fig. 2,  $R = 7$  cells, in Figs. 3 and 4,  $R = 6.7$  cells, and in Fig. 5, we used different values for  $R$ —see also description of Supplementary Movies). We numerically integrated the ordinary differential equations using fourth-order Runge-Kutta method and the diffusion and decay of IL-1 $\beta$  with a FTCS (forward in time centered in space). We solved the decay of IL-1 $\beta$  within the FTCS scheme because the cytokine decays everywhere on the grid. We applied absorbing (Dirichlet) boundary conditions to the cells at the perimeter of the grid by setting them to a constant low IL-1 level to simulated diffusion of IL-1 into the bloodstream. Notice that the hexagonal grid calculates the second derivative along

three axes. In 2D, diffusion only consists of two derivatives, therefore we multiply the FTCS terms by 2/3.

### Analysis of simulation data

We performed Kolmogorov-Smirnov test using Matlab's built-in function `kstest2`. The test has the benefit that it makes no assumption on the underlying pdf.

In Figs. 2C, D, 4A, B, 5A–C and Supplementary Fig. S5, the transitions of islets to locked state were fitted to a sigmoidal function:  $f(x) = \frac{1}{1 + \exp((x-a)/b)}$ , where  $a$  is the  $EC_{50}$ -value, where 50% percent of the islets are in the persistent mode.

### Data availability

All simulation data presented in this paper was generated by integrating the Eqs. (1)–(4) as described in the main text. The experimental data shown in Fig. 3 is available in ref. 37.

Received: 3 April 2024; Accepted: 19 August 2024;

Published online: 12 September 2024

### References

- Nair, V. D. et al. Early single cell bifurcation of pro- and antiapoptotic states during oxidative stress. *J. Biol. Chem.* **279**, 27494–27501 (2004).
- Albeck, J. G. et al. Quantitative analysis of pathways controlling extrinsic apoptosis in single cells. *Mol. Cell* **30**, 11–25 (2008).
- Lerner, A. G. et al. IRE1 $\alpha$  induces thioredoxin-interacting protein to activate the NLRP3 inflammasome and promote programmed cell death under irremediable ER stress. *Cell Metab.* **16**, 250–264 (2012).
- Walter, P. & Ron, D. The unfolded protein response: from stress pathway to homeostatic regulation. *Science* **334**, 1081–1086 (2011).
- Shore, G. C., Papa, F. R. & Oakes, S. A. Signaling cell death from the endoplasmic reticulum stress response. *Curr. Opin. Cell Biol.* **23**, 143–149 (2011).
- Wei, Y., Sinha, S. & Levine, B. Dual role of JNK1-mediated phosphorylation of Bcl-2 in autophagy and apoptosis regulation. *Autophagy* **4**, 949–951 (2008).
- Vousden, K. H. & Prives, C. Blinded by the light: the growing complexity of p53. *Cell* **137**, 413–431 (2009).
- Purvis, J. E. et al. p53 dynamics control cell fate. *Science* **336**, 1440–1444 (2012).
- Bernstein, C. et al. DNA repair/pro-apoptotic dual-role proteins in five major DNA repair pathways: fail-safe protection against carcinogenesis. *Mutat. Res.* **511**, 145–178 (2002).
- Cheng, W. C. et al. Mitochondrial factors with dual roles in death and survival. *Oncogene* **25**, 4697–4705 (2006).
- Dickinson, B. C. & Chang, C. J. Chemistry and biology of reactive oxygen species in signaling or stress responses. *Nat. Chem. Biol.* **7**, 504–511 (2011).
- Lambeth, J. D. & Neish, A. S. Nox enzymes and new thinking on reactive oxygen: a double-edged sword revisited. *Annu. Rev. Pathol.* **9**, 119–45 (2013).
- Dinarello, C. A., Donath, M. Y. & Mandrup-Poulsen, T. Role of IL-1 $\beta$  in type 2 diabetes. *Curr. Opin. Endocrinol. Diabetes Obes.* **17**, 314–321 (2010).
- Donath, M. Y. et al. Cytokine production by islets in health and diabetes: cellular origin, regulation and function. *Trends Endocrinol. Metab.* **21**, 261–267 (2010).
- Ehnes, J. A. et al. Increased number of islet-associated macrophages in type 2 diabetes. *Diabetes* **56**, 2356–2370 (2007).
- Boeni-Schnetzler, M. et al. IL-1 $\beta$  expression in human islets is induced by glucose and autostimulation, and increased in  $\beta$  cells of individuals with type 2 diabetes. *Diabetologia* **50**, S178 (2007).
- Mandrup-Poulsen, T., Pickersgill, L. & Donath, M. Y. Blockade of interleukin 1 in type 1 diabetes mellitus. *Nat. Rev. Endocrin.* **6**, 158–166 (2010).
- Bosco, D. et al. Unique arrangement of  $\alpha$ - and  $\beta$ -cells in human islets of Langerhans. *Diabetes* **59**, 1202–1210 (2010).
- Elayat, A. A., el-Naggar, M. M. & Tahir, M. An immunocytochemical and morphometric study of the rat pancreatic islets. *J. Anat.* **186**, 629–637 (1995).
- Steiner, D. J. et al. Pancreatic islet plasticity: interspecies comparison of islet architecture and composition. *Islets* **2**, 135–145 (2010).
- Winter, K. D. et al. Effects of glucose-dependent insulinotropic polypeptide on the phosphorylation of protein kinase B (PKB/AKT) and its contribution to pancreatic  $\beta$ -cell survival. *J. Invest. Med.* **55**, S76 (2007).
- Larsen, C. M. et al. Interleukin-1-receptor antagonist in type 2 diabetes mellitus. *N. Engl. J. Med.* **356**, 1517–1526 (2007).
- Boni-Schnetzler, M. et al. Flp stimulates angiogenic CXC-chemokine GRO/KC expression in insulin producing cells. *Diabetes* **56**, A413 (2007).
- Kilimnik, G. et al. Altered islet composition and disproportionate loss of large islets in patients with type 2 diabetes. *PLoS ONE* **6**, e27445 (2011).
- Youm, Y. H. et al. Elimination of the NLRP3-ASC inflammasome protects against chronic obesity-induced pancreatic damage. *Endocrinology* **152**, 4039–4045 (2011).
- Chabosseau, P. et al. Molecular phenotyping of single pancreatic islet leader  $\beta$  cells by “Flash-Seq”. *Life Sci.* **316**, p121436 (2023).
- Yde, P. et al. Modeling the NF- $\kappa$ B mediated inflammatory response predicts cytokine waves in tissue. *BMC Syst. Biol.* **5**, 115 (2011).
- Jo, J. et al. Formation of pancreatic islets involves coordinated expansion of small islets and fission of large interconnected islet-like structures. *Biophys. J.* **101**, 565–574 (2011).
- Yde, P., Jensen, M. H. & Trusina, A. Analyzing inflammatory response as excitable media. *Phys. Rev. E* **84**, 051913 (2011).
- Maedler, K. et al. Glucose-induced  $\beta$  cell production of IL-1 $\beta$  contributes to glucotoxicity in human pancreatic islets. *J. Clin. Invest.* **110**, 851–860 (2002).
- Goodhill, G. J. Diffusion in axon guidance. *Eur. J. Neurosci.* **9**, 1414–1421 (1997).
- Moran, A. et al. Interleukin-1 antagonism in type 1 diabetes of recent onset: two multicentre, randomised, double-blind, placebo-controlled trials. *Lancet* **381**, 1905–1915 (2013).
- Ashall, L. et al. Pulsatile stimulation determines timing and specificity of NF- $\kappa$ B-dependent transcription. *Science* **324**, 242–246 (2009).
- Ortiz, F. et al. Induction of nuclear factor- $\kappa$ B and its downstream genes by TNF- $\alpha$  and IL-1 $\beta$  has a pro-apoptotic role in pancreatic  $\beta$  cells. *Diabetologia* **51**, 1213–1225 (2008).
- Esser, N. et al. Inflammation as a link between obesity, metabolic syndrome and type 2 diabetes. *Diabetes Res. Clin. Pract.* **105**, 141–150 (2014).
- Donath, M. Y. & Shoelson, S. E. Type 2 diabetes as an inflammatory disease. *Nat. Rev. Immunol.* **11**, 98–107 (2011).
- Palmer, J. P. et al. Interaction of  $\beta$ -cell activity and IL-1 concentration and exposure time in isolated rat islets of Langerhans. *Diabetes* **38**, 1211–1216 (1989).
- Sprinkel, A. M., Andersen, N. A. & Mandrup-Poulsen, T. Glucose potentiates interleukin-1  $\beta$  (IL-1  $\beta$ )-induced p38 mitogen-activated protein kinase activity in rat pancreatic islets of Langerhans. *Eur. Cytokine Netw.* **12**, 331–339 (2001).
- Cavelti-Weder, C. et al. Effects of gevokizumab on glycemia and inflammatory markers in type 2 diabetes. *Diabetes Care* **35**, 1654–1662 (2012).
- Larsen, C. M. et al. Sustained effects of interleukin-1 receptor antagonist treatment in type 2 diabetes. *Diabetes Care* **32**, 1663–1668 (2009).

41. Donath, M. Y. Multiple benefits of targeting inflammation in the treatment of type 2 diabetes. *Diabetologia* **59**, 679–682 (2016).
42. Ramsden, L. & Rider, C. C. Selective and differential binding of interleukin (IL)-1  $\alpha$ , IL-1  $\beta$ , IL-2 and IL-6 to glycosaminoglycans. *Eur. J. Immunol.* **22**, 3027–3031 (1992).
43. Dahllof, M. S. et al. The lysine deacetylase inhibitor Givinostat inhibits  $\beta$ -cell IL-1 $\beta$  induced IL-1 $\beta$  transcription and processing. *Islets* **4**, 417–422 (2012).
44. O'Neill, C. M. et al. Circulating levels of IL-1B+IL-6 cause ER stress and dysfunction in islets from prediabetic male mice. *Endocrinology* **154**, 3077–3088 (2013).
45. Berchtold, L. A. et al. Cytokines and pancreatic  $\beta$ -cell apoptosis. *Adv. Clin. Chem.* **75**, 99–158 (2016).
46. Zhao, G. et al. Possible role of interleukin-1 $\beta$  in type 2 diabetes onset and implications for anti-inflammatory therapy strategies. *PLoS Comput. Biol.* **10**, e1003798 (2014).
47. Palmer, R. et al. Effects of IL-1 $\beta$ -blocking therapies in type 2 diabetes mellitus: a quantitative systems pharmacology modeling approach to explore underlying mechanisms. *CPT Pharmacomet. Syst. Pharm.* **3**, e118 (2014).
48. Tamassia, N. et al. Uncovering an IL-10-dependent NF- $\kappa$ B recruitment to the IL-1ra promoter that is impaired in STAT3 functionally defective patients. *FASEB J.* **24**, 1365–1375 (2010).
49. Huang, H. Y. et al. Interleukin (IL)-1 $\beta$  regulation of IL-1 $\beta$  and IL-1 receptor antagonist expression in cultured human endometrial stromal cells. *J. Clin. Endocrinol. Metab.* **86**, 1387–1393 (2001).
50. Skundric, D. S., Bealmeier, B. & Lisak, R. P. Induced upregulation of IL-1, IL-1RA and IL-1R type I gene expression by Schwann cells. *J. Neuroimmunol.* **74**, 9–18 (1997).
51. Maedler, K. et al. Leptin modulates  $\beta$  cell expression of IL-1 receptor antagonist and release of IL-1 $\beta$  in human islets. *Proc. Natl Acad. Sci. USA* **101**, 8138–8143 (2004).
52. Striegel, D. A., Hara, M. & Perival, V. The  $\beta$  cell in its cluster: stochastic graphs of  $\beta$  cell connectivity in the islets of Langerhans. *PLoS Comput. Biol.* **11**, e1004423 (2015).
53. Smolen, P., Rinzel, J. & Sherman, A. Why pancreatic islets burst but single  $\beta$  cells do not. The heterogeneity hypothesis. *Biophys. J.* **64**, 1668–1680 (1993).
54. Chirieleison, S. M. et al. Pattern transformation with DNA circuits. *Nat. Chem.* **5**, 1000–1005 (2013).
55. Silva, P. N. et al. A microfluidic device designed to induce media flow throughout pancreatic islets while limiting shear-induced damage. *Lab Chip* **13**, 4374–4384 (2013).
56. Roscioni, S. et al. Impact of islet architecture on  $\beta$ -cell heterogeneity, plasticity and function. *Nat. Rev. Endocrinol.* **12**, 695–709 (2016).
57. Benninger, R. K. P. & Kravets, V. The physiological role of  $\beta$ -cell heterogeneity in pancreatic islet function. *Nat. Rev. Endocrinol.* **18**, 9–22 (2022).
58. Aldous, N., Moin, A. S. M. & Abdelalim, E. M. Pancreatic  $\beta$ -cell heterogeneity in adult human islets and stem cell-derived islets. *Cell. Mol. Life Sci.* **80**, 176 (2023).
59. Brough, D. & Rothwell, N. J. Caspase-1-dependent processing of pro-interleukin-1 $\beta$  is cytosolic and precedes cell death. *J. Cell Sci.* **120**, 772–781 (2007).
60. Xia, S. et al. Gasdermin D pore structure reveals preferential release of mature interleukin-1. *Nat.* **593**, 607–611 (2021).
61. Werner, S. L. et al. Encoding NF- $\kappa$ B temporal control in response to TNF: distinct roles for the negative regulators I $\kappa$ B $\alpha$  and A20. *Genes Dev.* **22**, 2093–2101 (2008).
62. Jenkins, J. K. & Arend, W. P. Interleukin 1 receptor antagonist production in human monocytes is induced by IL-1  $\alpha$ , IL-3, IL-4 and GM-CSF. *Cytokine* **5**, 407–415 (1993).
63. Kondo, S. et al. Differential modulation of interleukin-1  $\alpha$  (IL-1  $\alpha$ ) and interleukin-1  $\beta$  (IL-1  $\beta$ ) in human epidermal keratinocytes by UVB. *Exp. Dermatol.* **3**, 29–39 (1994).
64. Turner, M. et al. Regulation of expression of human IL-1  $\alpha$  and IL-1  $\beta$  genes. *J. Immunol.* **143**, 3556–3561 (1989).
65. Moors, M. A. & Mizel, S. B. Proteasome-mediated regulation of interleukin-1 $\beta$  turnover and export in human monocytes. *J. Leukoc. Biol.* **68**, 131–136 (2000).
66. Kudo, S. et al. Clearance and tissue distribution of recombinant human interleukin 1 $\beta$  in rats. *Cancer Res.* **50**, 5751–5755 (1990).

### Acknowledgements

A.T. and M.H.J. acknowledge support from StemPhys DNRFCenter of Excellence (DNRFC116). M.H.J. acknowledges Novo Nordisk Foundation grants NNF20OC0064978 and NNF24OC0089788.

### Author contributions

A.T., T.M.P. and M.H.J. conceived the project. P.Y.N. and T.H.H. developed the model, performed simulations and analysis. A.T., T.H.H. and P.Y.N. wrote the original draft. All authors have contributed to the discussions at all stages, from model building to data analysis, and all have contributed to multiple rounds of revisions of the manuscript.

### Competing interests

The authors declare no competing interests.

### Additional information

**Supplementary information** The online version contains supplementary material available at <https://doi.org/10.1038/s41540-024-00427-4>.

**Correspondence** and requests for materials should be addressed to Mogens H. Jensen, Thomas Mandrup-Poulsen or Ala Trusina.

**Reprints and permissions information** is available at <http://www.nature.com/reprints>

**Publisher's note** Springer Nature remains neutral with regard to jurisdictional claims in published maps and institutional affiliations.

**Open Access** This article is licensed under a Creative Commons Attribution-NonCommercial-NoDerivatives 4.0 International License, which permits any non-commercial use, sharing, distribution and reproduction in any medium or format, as long as you give appropriate credit to the original author(s) and the source, provide a link to the Creative Commons licence, and indicate if you modified the licensed material. You do not have permission under this licence to share adapted material derived from this article or parts of it. The images or other third party material in this article are included in the article's Creative Commons licence, unless indicated otherwise in a credit line to the material. If material is not included in the article's Creative Commons licence and your intended use is not permitted by statutory regulation or exceeds the permitted use, you will need to obtain permission directly from the copyright holder. To view a copy of this licence, visit <http://creativecommons.org/licenses/by-nc-nd/4.0/>.

© The Author(s) 2024